Available online at www.sciencedirect.com

ScienceDirect

Proceedings of the Combustion Institute 37 (2019) 2911–2918

Proceedings of the Combustion Institute

www.elsevier.com/locate/proci

Investigating particle and volatile evolution during pulverized coal combustion using high-speed digital in-line holography

Longchao Yao [a,b], Chenyue Wu [a], Yingchun Wu [a], Linghong Chen [a], Jun Chen [b], Xuecheng Wu [a,*], Kefa Cen [a]

[a] *State Key Laboratory of Clean Energy Utilization, Zhejiang University, Hangzhou 310027, China*
[b] *School of Mechanical Engineering, Purdue University, West Lafayette, Indiana 47907, USA*

Received 1 December 2017; accepted 22 June 2018
Available online 7 July 2018

Abstract

Devolatilization is an important process in pulverized coal combustion because it affects the ignition, volatile combustion, and subsequent char burning and ash formation. In this study, high-speed digital in-line holography is employed to visualize and quantify the particle and volatile evolution during pulverized coal combustion. China Shanxi bituminous coal particles sieved in the range of 105–154 μm are entrained into a flat flame burner through a central tube for the study. Time-resolved observations show the volatile ejection, accumulation, and detachment in the early stage of coal combustion. Three-dimensional imaging and automatic particle extraction algorithm allow for the size and velocity statistics of the particle and stringy volatile tail. The results demonstrate the smaller particle generation and coal particle swelling in the devolatilization. It is found that the coal particles and volatiles accelerate due to the thermal buoyancy and the volatiles move faster than the coal particles. On average, smaller particles move faster than the larger ones while some can move much slower possibly because of the fragmentation.

Keywords: Coal devolatilization; High-speed digital in-line holography; Particle and volatile; Evolution

1. Introduction

The devolatilization in the early stage of pulverized coal combustion plays an important role in the whole combustion process because it not only determines the volatile release and combustion, but also has a significant influence on the subsequent char combustion and ash formation. A number of models have been developed to describe the devolatilization process including volatile yield and combustion, particle morphology evolution, etc. [1,2]. These phenomena were also observed directly via shadowgraphy [3], flame radiation imaging [4–6] and holography [7–9]. In the devolatilization, bubbles of the volatiles swell the softened coal particle and the particle size increases, together

* Corresponding author.
E-mail address: wuxch@zju.edu.cn (X. Wu).

https://doi.org/10.1016/j.proci.2018.06.179
1540-7489

with the porous structure formation. The released volatiles firstly burn around the parent particle and then gradually accumulate into stringy wake plume, which could detach from the particle before the oxidation. It is claimed that the condensed-phase volatiles ejected from the bituminous coal particles result from the pyrolytic cracking of the heavy hydrocarbons and relate to the soot formation [3,8]. Lignites, on the other hand, mostly produce CO, CO_2, H_2O, H_2 and light hydrocarbon gases in the devolatilization such that no evident condensed-phase volatile can be observed. That means bright-background imaging techniques like shadowgraphy and holography work better in observations of bituminous coal combustion. Image of flame radiation and particle incandescence is not limited by the gas transparency, but requires the object to be luminous that is not always the case for the combustion products.

Nevertheless, direct observation remains one of the most effective methods to study the early stage of coal combustion, especially when the high-speed camera is employed for time-resolved observation. Single coal particle behaviors in a drop tube furnace and the post-combustion gas of a flat flame burner, which simulate the high temperature and high heating rate environment in industrial applications, have been widely studied using high-speed videography [5,10–14]. Khatami et al. [10,11] observed the particle and flame evolution in the ignitions with different coal ranks. Bright envelope volatile flame around the bituminous coal particle followed with char burnout was observed, but the lignite burned with extensive fragmentation together with smaller scale volatile combustion. Lee and Choi [5,12] analyzed the wake flame feature and particle motion when a bituminous coal particle was entrained into a hot gas flow, and calculated the average results of more than 20 videos for each condition to ensure results were reliable and repeatable. It is difficult to study the individual particle within a particle cloud with the traditional imaging due to the narrow depth of field.

Digital in-line holography (DIH) proves to be effective in characterizing burning fuel particles [9,15,16]. It has the ability to quantify individual particle's behaviors in a global three-dimensional (3D) flow field. The 3D imaging feature of DIH allows for accurate measurements of particles in a volume with a relatively large depth of field. The volatile matter ejected from the particle in the devolatilization process appears to be a condensed phase, and thus can be clearly observed as a dark cloud by DIH. In addition, multiple particle parameters (e.g., size, morphology, concentration, 3D velocity) can be addressed simultaneously via DIH, while to achieve this, a combination of several different techniques such as high-speed video, particle image velocimetry/particle streak velocimetry, and scanned electron microscopy is required, as in [17].

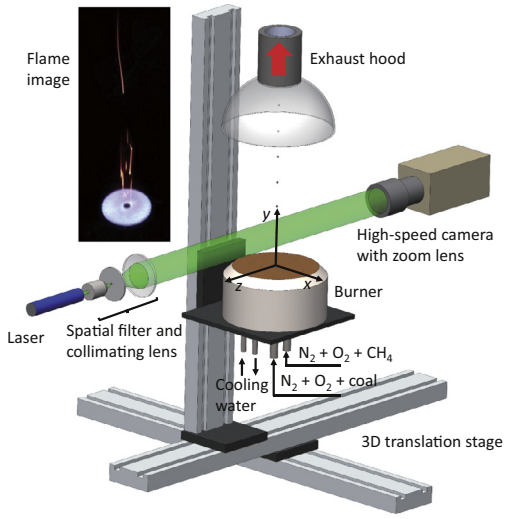

Fig. 1. Schematic of experimental setup for coal particle measurement with DIH, with a photograph of typical burning coal particles and volatile flames.

This work focuses on the particle and volatile behaviors at the early stage of pulverized bituminous coal combustion in the post-combustion gas of a flat flame burner using DIH. Both the direct observation of consecutive images of the individual particles and the statistical results are obtained after the hologram reconstruction and automatic particle extraction. Size and velocity evolution of particles and volatiles are compared at different heights. That explains the small particle formation, and coal particle swelling and fragmentation during the devolatilization. It is helpful for understanding the devolatilization process and its effect on the subsequent processes.

2. Experimental

2.1. Combustion setup

Figure 1 shows the schematic of the experimental setup. A modified Mckenna burner was used to provide a hot gas environment for coal ignition and combustion. O_2 and N_2 were first mixed with 2.4 standard (298 K, 101,325 Pa) liters per minute (slpm) and 9.6 slpm, respectively. Two slpm of the mixture entrained the coal particles into the combustion environment through the central tube, the inner diameter of which was 7.7 mm. The pulverized coal particles were given by a syringe injector pushed by a stepping motor at a feeding rate of about 0.01 g/s. Two slpm CH_4 was premixed with the remaining part (10 slpm) of O_2/N_2 mixture before burning to provide the hot gas. The diameter of the flat flame area was 60 mm. Since we used DIH as our main diagnostic method, we did not use the

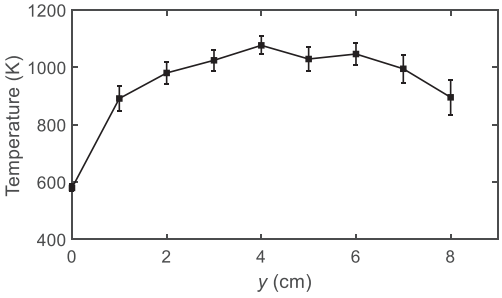

Fig. 2. Measured temperature by averaging results of three thermocouples at every 120° at the circumference of the central tube.

quartz chimney which was adopted in many other studies [5,18] to maintain the gas temperature, because even very small scratches on the quartz tube may severely affect the holographic fringes. Instead, gas temperature was maintained by providing excessive CH_4 in the fuel-oxygen mixture such that a small conical flame formed at the center of the burner, in addition to the flat flame. Then the gas temperature remained stably over 1000 K from 2.5 cm up to 6.5 cm above the burner, as shown in Fig. 2. Here we measured the gas temperature via three K-type thermocouples at every 120° at the circumference of the central tube and used the average value.

The burner was placed on a motorized 3D translation stage which was able to move different test sections into the field of view of DIH, as well as to adjust the recording distance. In this study, the highest test section went up to 7 cm above the burner, and the average residence time of the coal particles was about 50 ms.

2.2. Coal sample

China Shanxi bituminous coal was studied here because the volatiles released from bituminous coal are usually in a condensed phase and can be easily visualized in the reconstructed hologram. The proximate analysis (air-dried) showed 6.36% moisture, 21.29% ash, 28.13% volatile matter, and 44.22% fixed carbon. The coal particles were sieved to the size range of 105–154 μm.

2.3. High-speed DIH

3D imaging and quantification of individual coal particles as well as their volatiles were carried out using high-speed DIH. Figure 1 shows the implementation of the DIH system: A continuous wave laser (Oxxus LCX-532S, $\lambda = 532$ nm, 50–500 mW) was spatially filtered and collimated to a plane wave of 5 cm in diameter before traveling through the test section. The light scattered by the coal particles and volatiles was the object wave and the undisturbed part of the plane wave served as the reference wave. The object wave and the reference wave interfered to form the hologram that was recorded by the high-speed camera (Nac image technology, Memrecam HX-4). The camera was operated at 6000 frames per second (FPS) to record time-resolved holograms with exposure time of 2 μs, during which the particle displacements were smaller than 1/10 of their diameters. A lens (Nikon AF 50mm, 1:1.8D) with an adjustable bellow was mounted to the camera to magnify the hologram. A band-pass filter (532 ± 10 nm) was mounted before the camera, and it removed most of the flame radiation while allowing the laser light to reach the camera sensor. The hologram recorded with the lens system can be regarded as the magnified image of a virtual hologram at the front focal plane of the imaging system [19].

Particles were extracted from a hologram with the following steps: First, the hologram was volumetrically reconstructed between $z = -12$ mm and $z = 12$ mm (z is the depth location) in every 50 μm with the Fresnel diffraction formula [19]. Second, a depth-of-field extended image was synthesized using a wavelet-based image fusion algorithm [20]. Third, particles were segmented by applying a gray-scale threshold to the synthesized image. Finally, the z locations of the particles were determined with a focus metrics related to the variance of the intensity gradient in the vicinity of the particles. Then the 3D position, 2D morphology, and size of each particle were retrieved and saved. Further details including the selection of the threshold, the definition of the focus metrics, and the measurement accuracy of the algorithm could be found in [20,21].

3. Measurement uncertainty

Although the effectiveness and accuracy of DIH in particle measurement has been validated in previous researches [20,22], its application to coal combustion diagnostics is rare. The major cause of holographic image distortion, which could lead to subsequent measurement error, is the refractive index variation in the non-uniform high temperature environment. In order to evaluate its influences on the measurement accuracy, a tungsten wire was measured in conditions with and without the high temperature gas flow. The tungsten wire with two ends fixed was placed with a 3D tilt angle at 2 cm above the burner where the temperature reached about 1000 K. Measurements at room temperature are regarded as a reference.

A cropped reconstructed image in Fig. 3a shows that only a small section of the wire is focused at one reconstruction plane, and we obtained the 3D location and the diameter (local thickness indicated by the yellow arrows) of each section with an automated algorithm. The mean z locations and stan-

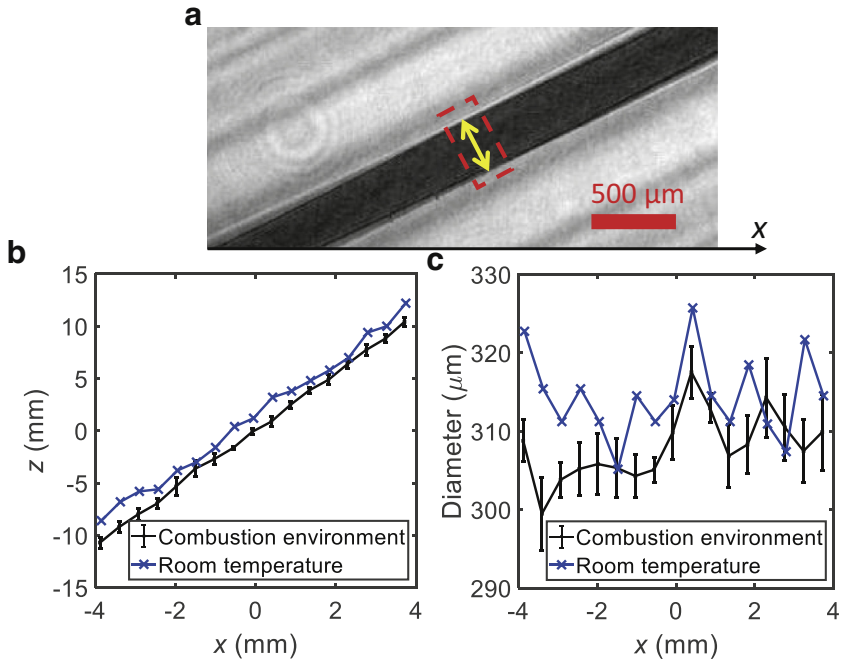

Fig. 3. Measurement uncertainty compared to the measurement at room temperature. (a) Demonstration of local z position and diameter extraction of the 3D tilted tungsten wire. (b) z location uncertainty. (c) Diameter uncertainty.

dard deviations along the x direction are calculated from the 13 frames (Fig. 3b). The z positions of the tungsten wire at high temperature shift about 1.5 mm compared to those at room temperature, but the similar $x - z$ linear features in the two cases indicate good accuracy in z locations. A global shift would not significantly affect the particle tracking and velocimetry. The small standard deviation (< 0.5 mm), on the other hand, proves the temporal stability, because the flame would not change much in this period. Fig. 3c shows the mean diameters and standard deviations of the wire at different positions. The mean diameter measured in the hot gas has similar fluctuations to that in the room temperature, with deviations smaller than 10 μm. Again there is a small overall shift (about 5 μm) between the two conditions with and without combustion.

4. Results and discussions

4.1. Observation of particle and volatile evolution

Figure 4 shows an example of denoised hologram and its reconstructed images that refocus different particles and volatile matters distributed in the 3D space. Figure 4a is a cropped hologram, and its reconstructed image at $z = -6$ mm is shown in Fig. 4b, and different structures and behaviors of the particles are observed in the image, with regions of interest magnified and refocused in Fig. 4c–4f. In Fig. 4c, the volatile matter was ejected to form a dark cloud and became denser within 2 ms. In most cases, the volatile gradually detached from the particle which then became bare char as shown in Fig. 4d. Then the volatile evolved into stringy structure, the length of which varies from hundreds of microns to several millimeters (Fig. 4f). Some coal particles also went through fragmentation in small scale according to the hologram video, as evidenced by the two small fragments in Fig. 4e, although this was not common in bituminous coal combustion.

Devolatilization occurred at about 5 ms after particles were entrained into the hot gas, and thus it was observed at the end of test section $0 < y < 1$ cm, and in the 1 cm $< y < 2$ cm section (the test sections were limited by the field of view: 7.9 mm width $\times$ 10.5 mm height). The whole devolatilization process (from volatile release to complete detachment) usually lasted 5–10 ms (see Fig. 5). The volatile matters came out of the particle and formed a dark cloud around the coal particle. Slip velocity between the particle and the gas made the volatile matter precede the parent particle, then accumulate to develop a condensed wake, and eventually detach from the particle after being elongated. The product of the devolatilization would either become long stringy objects or break up into small particles.

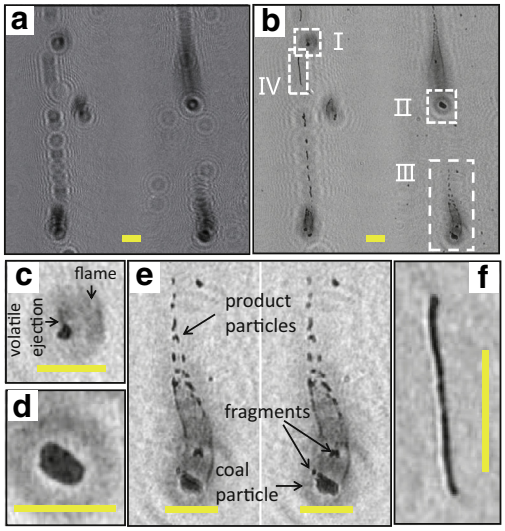

Fig. 4. Example of reconstructed hologram including typical phenomena of coal particle and released volatiles. (a) A cropped hologram and (b) its reconstruction at $z = -6$ mm. The regions enclosed in white boxes and labeled as I - IV are zoomed in and shown in (c)–(f), respectively. (c) volatile ejection. (d) bare char particle after volatile detaching. (e) small particles from volatile combustion and coal fragmentation (see the video). Note, (e) shows two reconstructed images at different z to refocus product particles and the coal particle. (f) stringy structure. The scale bar is 500 μm.

The intensity and shape of the condensed volatile change after being released, implying that it should be liquid or a cloud of small particles. In contrast, a particle fragmentation (e.g. in Fig. 4e) does not change its shape in a flexible way and is always opaque/dark. These two differences enable us to tell volatile from particle fragmentation. Mclean et al. [3] attributed the volatile cloud and tail to the formation and emission of the soot via pyrolysis of hydrocarbon volatiles. Seeker et al. [8] reported that the volatile cloud was from the agglomeration of homogeneously formed soot particles smaller than 50 nm. A higher magnification may help to find out more details of the condensed phase in the future but a single soot particle smaller than 50 nm is still difficult to be seen because of the optical resolution limitation. Alternatively, the amount of the soot might be evaluated with the area and intensity of the condensed phase. Higher intensity of the reconstructed image means higher transparency and lower soot density. As is shown in Fig. 5, the volatile cloud grows and becomes darker during the first 3 ms. It has the potential to characterize the soot formation rate in the homogeneous combustion.

4.2. Particle size evolution

Due to the co-existence of volatile matters and coal particles, the coal particles were first identified and separated from the volatile for particle size measurement, and here we used aspect ratio (major axis length divided by minor axis length) to distinguish the particle and volatile, because the volatile was usually elongated to a stringy object in the flow. Those with aspect ratio smaller than 3 were recognized as "particles" and larger than 5 were recognized as volatiles. It should be noted that the particle group could not exclude the small particles from the volatile cracking but the volatile group would not include coal or char particles with this criterion.

At each measurement section, 3000–5000 particles were extracted from 50 holograms to make the statistics. To avoid the recount of the same particle for the statistics, holograms were selected every 200

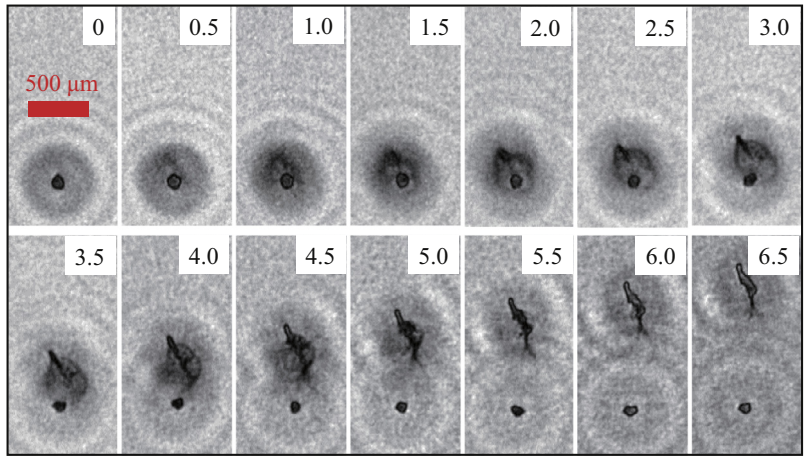

Fig. 5. The whole devolatilization visualized by sequential reconstructed images. The time at the top right corners has the unit of ms.

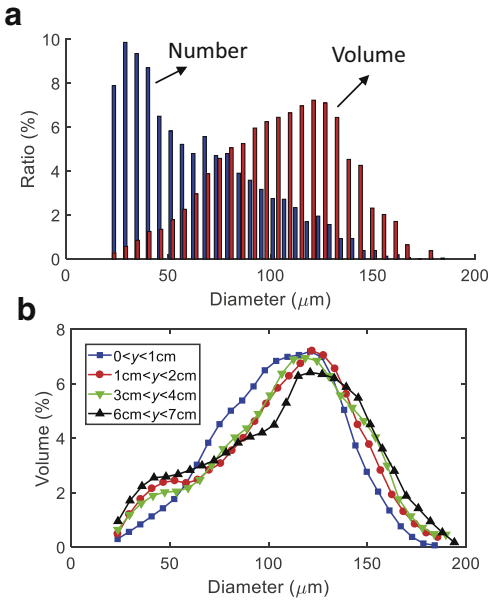

Fig. 6. Measured size distributions. (a) Number and volume fraction at $0 < y < 1$ cm section. (b) Comparison of volume fraction at four test sections.

sequential frames (33.3 ms), a period long enough for particles to leave the field of view. About 15,000 particles were detected and analyzed in total, and particle size ranged in 20–185 μm. Figure 6 shows the particle size distribution at the first test section ($0 < y < 1$ cm) and its evolution along the height direction. Though the coal particle were sieved to the size range of 105–154 μm, the number size distribution in Fig. 6a shows more smaller particles. That might be caused by the difficulty of removing all the small particles by sieving [23]. Sieving coal particles to a narrower size range may be better for the study on single particle combustion, but a relatively wide size range in this study match better to the particle cloud combustion in a real application. The volume size distribution provides a better understanding of particle size and its evolution. The peak and more than half of the volume are located between 105 μm and 154 μm. On the other hand, particle size would increase in the devolatilization when volatile bubbles were formed and caused the particle swelling. According to the previous studies [24,25], the fast swelling of a heated coal particle would be observed in the first 100 ms and the swelling ratio would vary with heating rate, coal rank, particle size, etc. That explains why some particles were measured up to 185 μm in size.

To further study the formation of small particle less than 70 μm and coal particle swelling, the volume size distributions at different heights are compared in Fig. 6b. The volume of center peak region with size from about 100 μm to 140 μm decreases, while particle volumes at the two sides

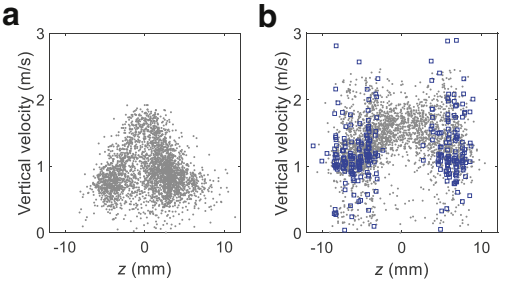

Fig. 7. Measured vertical velocity at (a) $0 < y < 1$ cm section and (b) 1 cm $< y < 2$ cm section. Gray dots represent the particle and blue squares represent stringy volatile. (For interpretation of the references to color in this figure legend, the reader is referred to the web version of this article.)

increase gradually with height. Volume size distributions at higher test sections tend to have a second peak at small size, i.e., about 40 μm, making the volume size distribution present a bimodal distribution. Combined with the direct observation of the particle and volatile evolution, the second peak of smaller particles results from the devolatilization products as described in Section 4.1. These smaller "particles" are totally opaque substances that are assumed to be soot agglomerations. They usually moved faster than the parent particles, which will be detailed in Section 4.3. The volume fraction of small particles increases obviously from $0 < y < 1$ cm region to 1 cm $< y < 2$ cm region, but does not change significantly at higher test sections. That means most of the coal particles released volatiles at the 1 cm $< y < 2$ cm region, in good agreement with the observations in Section 4.1. On the other hand, the curves that shift right for larger particles in Fig. 6 prove the particle swelling. This stable shift indicates that the swelling continued to the highest test section, and even after that, because the average residence time of the particles was only about 60 ms according to the particle velocity.

4.3. *Particle and volatile velocity*

The velocity of the particle and stringy volatile structure was calculated after being matched with the Hungarian algorithm [26]. Figure 7 compares the vertical velocity along the z direction (x direction was limited by the small field of view) at $0 < y < 1$ cm where no evident devolatilization was found, and at 1 cm $< y < 2$ cm where a large number of particles began to release volatiles. The velocity profile at the $0 < y < 1$ cm section (Fig. 7a) has a quasi-parabolic shape with the apex of 1.9 m/s. The particles were accelerated by the thermal buoyancy: The velocity of the hot post-combustion gas (~0.2 m/s at burner surface) with larger passage area was smaller than that of

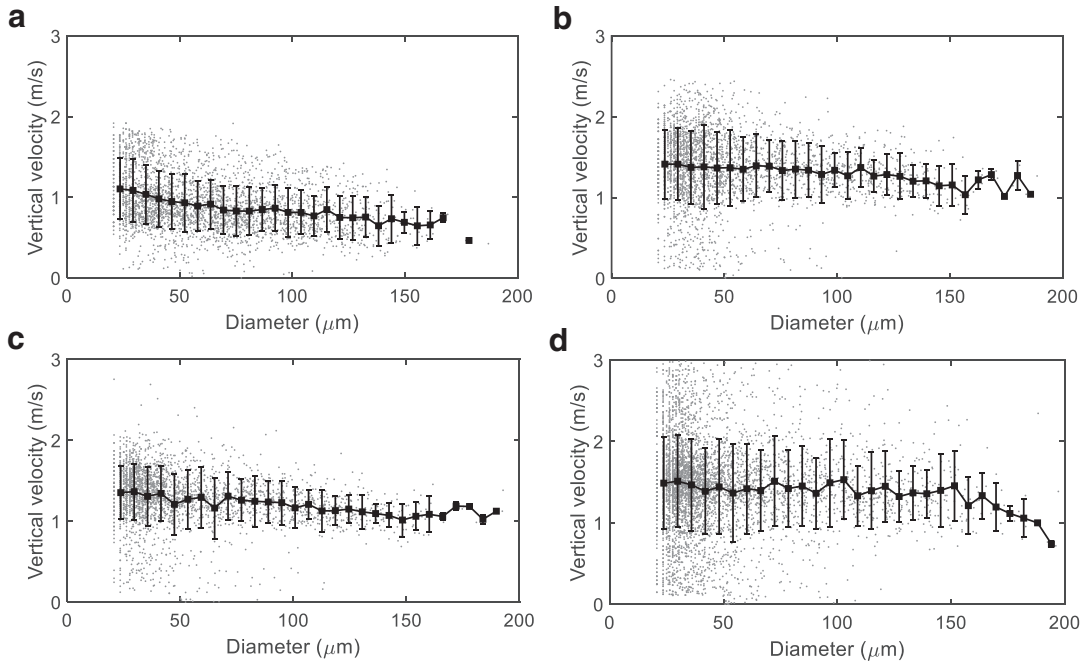

Fig. 8. Measured vertical velocity related with particle diameter at (a) $0 < y < 1$ cm section, (b) 1 cm $< y < 2$ cm section, (c) 3 cm $< y < 4$ cm section, and (d) 6 cm $< y < 7$ cm section. Gray dots are the measured data. Black dots and bars represent mean velocities and standard deviations.

the cold entraining gas (apex of $\sim$1.43 m/s regarded as a laminar pipe flow). However, the post-combustion gas heated the entraining gas to make it expand and move faster upward. The temperature increased rapidly with the height near the burner surface so that the velocity of the entraining gas also increased dramatically. The accelerated gas then dragged the particle and made it move faster upward. This acceleration also led to an overall larger particle velocity at 1 cm $< y < 2$ cm (Fig. 7b) compared to that at $0 < y < 1$ cm. Differently, many faster moving particles appeared near the edge at 1 cm $< y < 2$ cm, rather than at the center. That is because the volatiles evolved into small particles which moved faster than their parent coal particles. And the devolitilization happened only near the edge where the temperature was higher at this test section. Stringy volatile tails (labeled with blue squares), the velocity of which can be higher than the center particles, also appear only near the edge.

The relative velocity of a volatile tail was about 0.25 m/s to its parent particle from a limited number of instances. Some models and experimental results [27,28] showed that volatile flame could help trigger the char ignition via heat transfer. Char ignition happened when the ambient gas temperature was even lower than the ignition temperature with the particle burning in a quiescent environment (volatile flame was close to the particle). However, the velocity slip in this study, which also exists in a real boiler, will shorten the influence time of volatile flame on the particle. Whether the char particle can be ignited depends on the total energy it absorbs from the environment, and the volatile flame. The influence of flame location and lifespan on char combustion was not discussed in the previous works, but knowing the flame location is important to predict the lowest environment temperature to trigger char ignition. The velocity slip here will help the development of the model for the joint hetero-homogeneous ignition [27] in real applications, as well as the design of flow-combustion conditions.

The relationships between vertical velocities and particle sizes at different test sections are demonstrated in Fig. 8. On average, smaller particles moved faster than larger ones in all the four test sections because smaller particles can better follow the gas flow which provide the momentum of the particles. There is a significant acceleration from the $0 < y < 1$ cm section (Fig. 8a) to the 1 cm $< y < 2$ cm section (Fig. 8b) as is discussed in Fig. 7. The average velocity profiles remain similar in Figs. 8b–8d, but particle velocities are dispersed wider at higher test sections. The fastest small particles (from volatile cracking with small aspect ratios) moved as fast as 3 m/s. The reason why some small particles moved much slower than the larger particles (> 100 μm) is unclear. One interpretation is that small particles formed in the fragmentation were decelerated when the small fragments were at

the bottom of the parent particle. Note that only the upward-moving particles are taken into account here.

5. Conclusions

Particle and volatile behaviors in pulverized bituminous coal devolatilization are observed and quantified using DIH. Devolatilization started at about 1 cm above the burner for most coal particles. The released volatiles evolve into small particles or stringy structures and detach from the parent coal particle due to the gas-solid slip. Particle size statistics indicate that small particles formed as volatile product peak at about 40 μm, and the volume fraction of these particles will not change significantly at the higher places. Meanwhile the swelling of coal particles increases their sizes which happens all the time up to 7 cm above the burner. A velocity comparison of coal particles and volatiles along z direction between $0 < y < 1$ cm and 1 cm $< y < 2$ cm cases further proves the generation of small particles and the slip velocity. Particle acceleration is observed. Though the mean velocity of smaller particles are larger than that of larger particles, the former disperse in a much wider range. This may be the statistical evidence of fragmentation.

The observation and quantitative analysis of sequential holograms will help to understand the soot formation process and the influence of volatile flame on char combustion. It may also provide a method to improve and validate more accurate models for real applications, as well as improve the flow-combustion conditions. On the other hand, we are only able to get limited information in complex coal combustion with DIH. Many other key parameters such as temperature and composition of volatiles and particles can not be measured. To do this, other optical techniques may be used together with DIH (e.g. [16]) in the future.

Acknowledgments

This work was partially supported by National Natural Science Foundation of China (51576177), National Basic Research Program of China (2015CB251501), the program of introducing talents of discipline to universities (B08026), and China Scholarship Council (201606320173).

Supplementary material

Supplemental video is available to demonstrate the phenomena in Fig. 4 Supplementary material associated with this article can be found, in the online version, at doi:10.1016/j.proci.2018.06.179.

References

[1] G.-S. Liu, H. Rezaei, J. Lucas, D. Harris, T. Wall, *Fuel* 79 (14) (2000) 1767–1779.
[2] C. Sheng, J. Azevedo, *Proc. Combust. Inst.* 28 (2) (2000) 2225–2232.
[3] W. McLean, D. Hardesty, J. Pohl, in: Symp. (Int.) Combust., Vol. 18, Elsevier, 1981, pp. 1239–1248.
[4] C.R. Shaddix, A. Molina, *Proc. Combust. Inst.* 32 (2) (2009) 2091–2098.
[5] H. Lee, S. Choi, *Combust. Flame* 162 (6) (2015) 2610–2620.
[6] M. Xia, D. Zabrodiec, P. Scouflaire, B. Fiorina, N. Darabiha, *Proc. Combust. Inst.* 36 (2) (2017) 2123–2130.
[7] G.S. Samuelsen, J.D. Trolinger, M.P. Heap, W.R. Seeker, *Combust. Flame* 40 (1981) 7–12.
[8] W. Seeker, G. Samuelsen, M. Heap, J. Trolinger, in: Symp. Int. Combust., Vol. 18, Elsevier, 1981, pp. 1213–1226.
[9] Y. Wu, L. Yao, X. Wu, J. Chen, G. Gréhan, K. Cen, *Fuel* 206 (2017) 429–436.
[10] R. Khatami, C. Stivers, K. Joshi, Y.A. Levendis, A.F. Sarofim, *Combust. Flame* 159 (3) (2012a) 1253–1271.
[11] R. Khatami, C. Stivers, Y.A. Levendis, *Combust. Flame* 159 (12) (2012) 3554–3568.
[12] H. Lee, S. Choi, *Combust. Flame* 169 (2016) 63–71.
[13] C. Bu, D. Liu, X. Chen, D. Pallarès, A. Gómez-Barea, *Appl. Energy* 115 (2014) 301–308.
[14] R.-G. Kim, D. Li, C.-H. Jeon, *Eep. Therm. Fluid Sci.* 54 (2014) 212–218.
[15] Y. Wu, X. Wu, L. Yao, et al., *Fuel* 195 (2017) 12–22.
[16] Y. Chen, D.R. Guildenbecher, K.N. Hoffmeister, et al., *Combust. Flame* 182 (2017) 225–237.
[17] R. Rajasegar, D.C. Kyritsis, *J. Energ. Eng.* 141 (2) (2014) C4014012.
[18] A. Molina, C.R. Shaddix, *Proc. Combust. Inst.* 31 (2) (2007) 1905–1912.
[19] J. Sheng, E. Malkiel, J. Katz, *Appl. Opt.* 45 (16) (2006) 3893–3901.
[20] Y. Wu, W. Xuecheng, J. Yang, et al., *Appl. Opt.* 53 (4) (2014) 556–564.
[21] L. Yao, X. Wu, Y. Wu, et al., *Appl. Opt.* 54 (1) (2015) A23–A31.
[22] J. Katz, J. Sheng, *Ann. Rev. Fluid Mech.* 42 (2010) 531–555.
[23] Y. Chen, G. Wang, C. Sheng, *Energy & Fuels* 28 (1) (2013) 136–145.
[24] J. Yu, J.A. Lucas, T.F. Wall, *Prog. Energy Combust. Sci.* 33 (2) (2007) 135–170.
[25] H. Gao, S. Murata, M. Nomura, M. Ishigaki, M. Qu, M. Tokuda, *Energy fuels* 11 (3) (1997) 730–738.
[26] G. Fielding, M. Kam, in: 36th IEEE Conference on Decision and Control, 1997, vol. 2, IEEE, 1997, pp. 1928–1933.
[27] J. Yu, M.-c. Zhang, J. Zhang, *Proc. Combust. Inst.* 32 (2) (2009) 2037–2042.
[28] K. Li, C. You, *Energy & Fuels* 24 (8) (2010) 4178–4184.